Adaptive Model-Based Segmentation of Human Vessels from 3D MRA and CTA Data

Stefan Wörz and Karl Rohr

University of Heidelberg and DKFZ Heidelberg,
iBioS, Biomedical Computer Vision Group,
Im Neuenheimer Feld 580, 69120 Heidelberg, Germany
Email: {s.woerz, k.rohr}@dkfz.de

Abstract. We introduce an adaptive model fitting approach for the segmentation of human vessels from 3D images. The shape and size of the region-of-interest (ROI) used for model fitting are automatically adapted to the local width, curvature, and orientation of the vessel to increase the robustness and accuracy of model fitting. In conjunction with our previously proposed cylindrical model, the new adaptive approach has been successfully applied to segment vessels from 3D MRA and CTA images. Our experiments show that the adaptive approach yields superior segmentation results compared to approaches based on a fixed size ROI.

1 Introduction

Segmentation and quantification of vessels from 3D medical images is crucial for diagnosis, treatment, and surgical planning. In clinical practice, images of the human vascular system are acquired using different imaging modalities, for example, 3D magnetic resonance angiography (MRA) or computed tomography angiography (CTA). However, the segmentation of vessels from 3D medical images is difficult and challenging for several reasons: The width of vessels depends on the type of vessel, the width typically varies along vessels, the images are noisy, and the boundaries between the vessels and surrounding tissues are locally difficult to recognize, in particular, when considering curved 3D structures.

Previous work on the segmentation of vessels from 3D image data can be divided into two main classes of approaches, one based on differential measures (e.g., [1]) and the other based on deformable models (e.g., [2]). The main disadvantage of differential measures is that only local image information is taken into account. On the other hand, approaches based on deformable models generally exploit *contour* information of the anatomical structures. While these approaches include more global information in comparison to differential approaches, only 2D or 3D contours are taken into account. Alternatively, deformable models using *intensity* models have been suggested (e.g., [3, 4]). In comparison to previous contour-based models more image information is taken into account to improve the robustness and accuracy of the segmentation result. With these approaches a fitting scheme is employed where the model is directly fitted to the image intensities within region-of-interests (ROIs). However, these approaches use ROIs

with a *fixed* size along the whole vessel. This can lead to inaccurate estimates of the vessel's width for two reasons. First, the width of vessels generally varies along the vessel and therefore a fixed size ROI is not optimal for the whole vessel. If the ROI is too large it might contain neighboring structures which negatively influence the accuracy. On the other hand, if the ROI is too small the estimated results are not reliable. Second, the curvature of vessels also often varies along a vessel. As these approaches are based on straight models (e.g., straight cylinder segments) they can only approximate curved structures (by using a ROI in axial direction along the cylinder). Again, using a fixed size ROI is not optimal for the whole vessel, i.e. if the ROI is too large the model cannot well approximate the curved vessel, and if the ROI is too small the model is more sensitive to noise.

We have developed a new adaptive model fitting approach where the size and shape of the ROI are automatically *adapted* to the local width, curvature, and orientation of the vessel. We propose two independent schemes. First, the ROI size in axial direction (along the vessel) is adapted to the local curvature of the vessel, i.e. an increasing curvature along the vessel results in a shortening of the ROI and vice versa. As a result, the ROI in axial direction is reduced to allow a good approximation of a curved vessel but can also be extended to include more image information to decrease the influence of noise in case of low curvature parts. Second, the ROI size in orthogonal direction is adapted to the local width of the vessel, i.e. an increasing width along the vessel results in an increasing width of the ROI and vice versa. As a result, the vessel is always well inside the ROI but neighboring structures are excluded as much as possible.

2 Adaptive Size and Shape of the ROI

To segment vessels from 3D image data we utilize an incremental process that starts from a given point of the vessel and proceeds along a certain direction. In each increment, the parameters of a vessel segment (radius R, contrast a, image blur σ, 3D position $\mathbf{x}_0$, and 3D orientation $\boldsymbol{\alpha}$) are determined by fitting a 3D parametric intensity model to the image intensities within a 3D ROI. Here, we use the cylindrical model $g_{M,Cylinder}$ proposed in [4] that is an approximation of a Gaussian smoothed cylinder and is well-suited for vessels of small, medium, and large sizes. Initial parameters for the fitting process are determined from the estimated parameters of the previous segment using a Kalman filter.

We adapt the size and shape of the 3D ROI based on the initial parameters of the current vessel segment. For each segment, a local coordinate system is defined where the origin and orientation are given by the 3D position and orientation of the vessel segment (see Fig. 1, left). In this coordinate system, the z-axis is pointing along the vessel (axial) and the x- and y-axes are pointing orthogonal to the vessel. Adaptive model fitting is realized using a spherical ROI and, in addition, applying a weighting function to the voxels inside the ROI. As weighting function we use a Gaussian where the argument is given by the z-coordinate of a voxel in the local coordinate system, i.e. $w(x,y,z) = \exp\left(-z^2/\left(2\sigma_w^2\right)\right)$. The weighting function emphasizes voxels closer to the xy-plane at the origin and

Fig. 1. 2D sketch of a curved vessel with decreasing width along the vessel and the adapted ROI for three segments (left). In addition, a 2D section of the 3D weighting function $w(x, y, z)$ for a ROI radius of $R_{ROI} = 10$ voxels and a standard deviation of $\sigma_w = 4$ voxels is shown (center). The sketch on the right shows the centerline of a curved vessel (bold arc) as well as two estimated positions $\mathbf{x}_1$ and $\mathbf{x}_2$ along with their orientations $\mathbf{v}_1$ and $\mathbf{v}_2$. The distance d and the change of direction δ as well as the radius R_κ defining the curvature κ of the arc are marked.

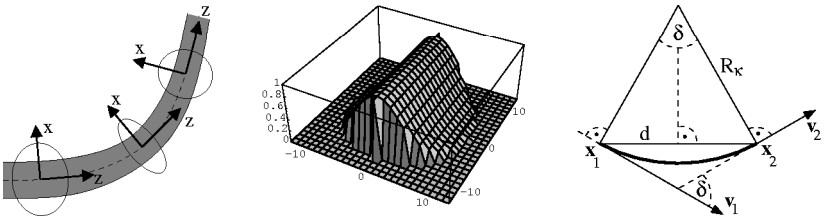

reduces the influence of voxels further away, resulting in an effective shortening of the ROI in axial direction (see Fig. 1, center). Thus, the ROI has an ellipsoidal (discus-like) shape. The shortening itself is controlled by the standard deviation σ_w of the Gaussian function, which is adapted to the local vessel curvature κ using

$$\sigma_w = c_{\sigma_w} + c_\kappa / \kappa \tag{1}$$

with constants c_{σ_w} and c_κ, where σ_w is restricted to a certain interval. This adaptation results in an optimal axial length of the ROI w.r.t. vessels of varying curvature. Here, the curvature κ is estimated based on the fitting results of the previous two vessel segments at positions $\mathbf{x}_1$ and $\mathbf{x}_2$ (see Fig. 1, right). The change of direction δ between the estimated (normalized) orientations $\mathbf{v}_1$ and $\mathbf{v}_2$ is given by $\delta = \arccos(\langle \mathbf{v}_1, \mathbf{v}_2 \rangle)$ where $\langle \cdot, \cdot \rangle$ denotes the inner product. Using the Euclidean distance d between $\mathbf{x}_1$ and $\mathbf{x}_2$, κ computes to $\kappa = R_\kappa^{-1} = 2\, d^{-1} \sin(\delta/2)$. The second adaptation mechanism is achieved by controlling the size of the spherical ROI itself. The radius R_{ROI} of the sphere is adapted to the local vessel radius R and image blur σ by

$$R_{ROI} = \lfloor c_R\, R + c_\sigma\, \sigma + c + 0.5 \rfloor \tag{2}$$

using constants c_R, c_σ, and c, and the floor function $\lfloor \cdot \rfloor$. This results in an optimal orthogonal ROI size, and thus we can cope with vessels of varying width.

3 Experimental Results

We have applied our new adaptive model fitting approach using a large spectrum of different 3D synthetic images as well as 3D MRA and CTA images.

First, we determined values for the constants in (2) that yield optimal adaptations of the ROI size. We created 168 different synthetic images of straight cylinders by varying the radius ($R = 1, \ldots, 7$ voxels), the image blur ($\sigma = 0.5, 1, \ldots, 3$ voxels), and the noise level. For each cylinder, we used 6 different ROI radii,

Fig. 2. The differences of the estimated radius (mean, minimum, and maximum for 110 to 224 segments) and the true radius $R = 3$ voxels of the cylindrical cross section of a torus are shown for different torus radii R_κ using a fixed size ROI (left) and an adaptive ROI (right). The dashed lines highlight the error interval of ± 0.1 voxels.

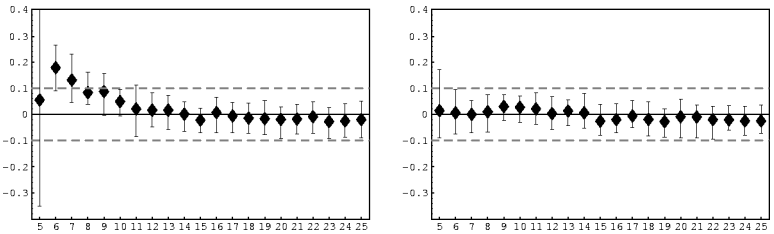

thus we conducted about 1000 experiments. Here, we did not apply the weighting function. From the segmentation results (not shown here) it turned out that $c_R = 1$, $c_\sigma = 2$, and $c = 2$ give accurate estimates in nearly all experiments.

Second, we determined values for the constants in (1) that result in optimal adaptations of the ROI shape. We created 315 different synthetic images of tori by varying the torus radius ($R_\kappa = 5, \ldots, 25$ voxels, i.e. $\kappa = 0.2, \ldots, 0.04$), the radius of the cylindrical cross-section ($R = 1, \ldots, 5$ voxels), and the noise level. For each torus, we used 16 different standard deviations of the weighting function ($\sigma_w = 0.5, 1, \ldots, 8$ voxels), thus we conducted about 5000 experiments. The segmentation results suggest that $c_{\sigma_w} = -8/3$ and $c_\kappa = 2/3$ in combination with $2 \leq \sigma_w \leq 6$ yield accurate fitting results. For example, Fig. 2 summarizes the segmentation results of 21 tori for different torus radii R_κ. Shown are the errors of the estimated radius R using a fixed size (left) as well as an adaptive ROI (right) for vessel segmentation. It can be seen that the adaptive ROI yields quite accurate results and significantly improves the accuracy of the estimated radius for larger curvatures (particularly see the *left part* of both diagrams).

Third, we carried out experiments based on 205 synthetic images containing different tubular structures of varying width and curvature (i.e. 3D spirals and cylinders with a variable radius along the cylinder). We found that the new approach is quite robust against noise and produces significantly more accurate results in comparison to the previous approach. For example, Fig. 3 shows the segmentation result of a screw-like 3D spiral with a radius of $R = 2$ voxels (left). In addition, the estimated radius along the spiral is shown for a fixed size (grey) as well as an adaptive ROI (black). It turns out that using an adaptive ROI yields accurate results, i.e. the maximal error of the estimated radius is below 0.11 voxels for the first four windings and below 0.26 voxels for the last part (where the curvature is very large). In contrast, the previous approach yields a maximal error of up to 0.39 voxels for the first four windings, and is not able to fully segment the last part (errors up to 0.7 voxels for the segmented part).

Finally, from the experiments based on real 3D images it turns out that the adaptive approach successfully segments and quantifies arteries of different sizes and high curvatures. For example, Fig. 4 shows the segmentation results of the aorta (MRA, left) and of arteries of the thorax (CTA, right).

Fig. 3. Segmentation result of a screw-like 3D spiral with radius $R = 2$ (left). The right diagram shows the estimated radius for about 480 voxels along the spiral for a fixed size ROI (grey) and an adaptive ROI (black). The vertical lines separate the windings.

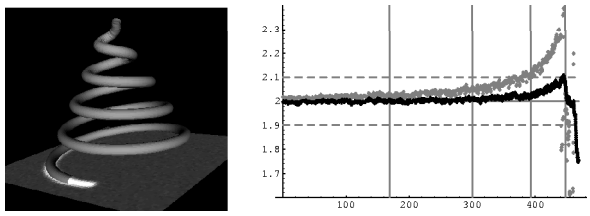

Fig. 4. Segmentation results of applying the new approach to the aorta (MRA, left) and to thorax arteries (CTA, right). For visualization we used 3D Slicer (SPL, Boston).

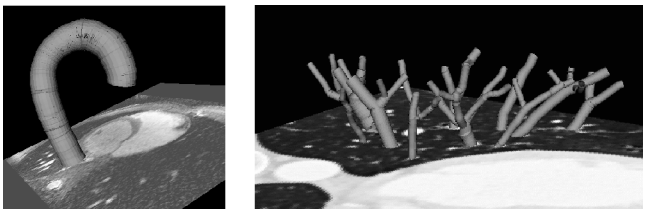

4 Discussion

We introduced a new adaptive model fitting approach for fitting a cylindrical intensity model to tubular structures. Experiments using synthetic and real 3D images show that the approach is quite robust against noise and produces significantly more accurate results for tubular structures of varying width and curvature in comparison to the previous approach using a fixed size ROI. The approach is well-suited for vessels of small, medium, and large widths as well as for vessels with varying width and curvature along the vessel.

Acknowledgement. The MRA image of the thorax has kindly been provided by Philips Research Laboratories Hamburg. The CTA image of the thorax is courtesy of Dr. med. T. Maier and Dr. C. Lienerth, Gemeinschaftspraxis Radiologie, Frankfurt/Main.

References

1. Krissian K, Malandain G, Ayache N, Vaillant R, Trousset Y. Model Based Detection of Tubular Structures in 3D Images. CVIU 2000;80(2):130–171.
2. Frangi AF, Niessen WJ, Hoogeveen RM, *et al.* Model-Based Quantitation of 3D Magnetic Resonance Angiographic Images. T-MI 1999;18(10):946–956.
3. Noordmans HJ, Smeulders AWM. High accuracy tracking of 2D/3D curved line structures by consecutive cross-section matching. PRL 1998;19(1):97–111.
4. Wörz S, Rohr K. A New 3D Parametric Intensity Model for Accurate Segmentation and Quantification of Human Vessels. In: MICCAI'04; 2004. p. 491–499.